

Tropospheric HONO Distribution and Chemistry in the Southeast U.S.

Chunxiang Ye^{1,2}, Xianliang Zhou^{2,3}, Dennis Pu³, Jochen Stutz⁴, James Festa⁴, Max Spolaor⁴, Catalina Tsai⁴, Christopher Cantrell⁵, Roy L. Mauldin III^{5,6}, Andrew Weinheimer⁷, Rebecca S. Hornbrook⁷, Eric C. Apel⁷, Alex Guenther⁸, Lisa Kaser⁷, Bin Yuan⁹, Thomas Karl¹⁰, Julie Haggerty⁷, Samuel Hall⁷, Kirk Ullmann⁷, James Smith^{7,11}, John Ortega⁷

[1] State Key Joint Laboratory of Environmental Simulation and Pollution Control, College of Environmental Sciences and Engineering, the Key Joint Laboratory of Environment

[2] Wadsworth Center, New York State Department of Health, Albany, NY

[3] Department of Environmental Health Sciences, State University of New York, Albany, NY

[4] Department of Atmospheric and Oceanic Sciences, University of California, Los Angeles, CA

[5] Department of Atmospheric and Oceanic Sciences, University of Colorado-Boulder, Boulder Colorado

[6] Department of Physics, University of Helsinki, Helsinki, Finland

[7] National Center for Atmospheric Research, Boulder, Colorado

[8] Department of Earth System Science, University of California, Irvine, CA

[9] Institute for Environmental and Climate Research, Jinan University, Guangzhou, 511443

[10] Institute of Atmospheric and Cryospheric Sciences, University of Innsbruck, Innsbruck, Austria

[11] University of Eastern Finland, Kuopio, Finland

Correspondence to: Chunxiang Ye (c.ye@pku.ed.u.cn) and Xianliang Zhou (xianliang.zhou@health.ny.gov)

1 **Abstract**

2 Here we report the measurement results of nitrous acid (HONO) and a suite of relevant
3 parameters on the NCAR C-130 research aircraft in the Southeast U.S. during the NOMADSS
4 2013 summer field study. The daytime HONO concentration ranged from low parts per
5 trillion by volume (pptv) in the free troposphere (FT) to mostly within 5 - 15 pptv in the
6 background planetary boundary layer (PBL). There was no discernible vertical HONO
7 gradient above the lower flight altitude of 300 m in the PBL, and the transport of ground
8 surface HONO was found not a significant contributor to the tropospheric HONO budget. The
9 total *in situ* HONO source, mean (± 1 SD) was calculated $53 (\pm 21)$ pptv h^{-1} during the day.
10 The upper limit contribution from NO_x -related reactions was $10 (\pm 5)$ pptv h^{-1} , and the
11 contribution from photolysis of particulate nitrate (pNO_3) was $38 (\pm 23)$ pptv h^{-1} , based on the
12 measured pNO_3 concentrations and the median pNO_3 photolysis rate constant of $2.0 \times 10^{-4} \text{ s}^{-1}$
13 determined in laboratory using ambient aerosol samples. The photolysis of HONO contributed
14 to less than 10% of the primary OH source. However, a recycling NO_x source via pNO_3
15 photolysis was equivalent to $\sim 2.3 \times 10^{-6} \text{ mol m}^{-2} \text{ h}^{-1}$ in the air column within the PBL, a
16 considerable supplementary NO_x source in the low- NO_x background area. Up to several tens
17 pptv of HONO were observed in power plant and urban plumes during the day, mostly
18 produced *in situ* from precursors including NO_x and pNO_3 . Finally, there was no observable
19 accumulation of HONO in the nocturnal residual layer and the nocturnal FT in the
20 background Southeast U.S., with an increase in HONO/ NO_x ratio of $\leq 3 \times 10^{-4} \text{ hr}^{-1}$ after
21 sunset.
22

23 1 Introduction

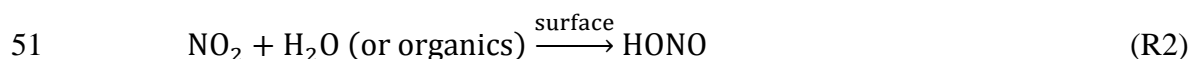
24 Extensive field studies at ground sites have shown that gas-phase nitrous acid (HONO)
25 exists at much higher levels than expected during the day, with a mixing ratio of HONO up to
26 several parts per billion by volume (ppbv) in the urban atmosphere (Acker et al., 2006;
27 Villena et al., 2011) and up to several hundred parts per trillion by volume (pptv) in rural
28 environments (Acker et al., 2006; Kleffmann et al., 2003; Zhang et al., 2009; Zhou et al.,
29 2002, 2011). At the observed concentrations, HONO photolysis (R1) becomes an important or
30 even a major OH primary source in both urban (Elshorbany et al., 2010; Villena et al., 2011)
31 and rural environments near the ground surface (Acker et al., 2006; He et al., 2006;
32 Kleffmann et al., 2003; Zhou et al., 2002, 2011).



34 The OH radical is responsible for the removal of primary pollutants, and plays a crucial role in
35 the formation of secondary pollutants, such as O₃ and aerosol (Finlayson-Pitts and Pitts,
36 2000), and thus HONO plays an important role in atmospheric chemistry.

37 The removal processes of HONO from the troposphere are relatively well understood,
38 including mainly photolysis, reaction with the OH radical and surface deposition. Photolysis
39 is the dominant sink for HONO during the day (Kleffmann et al., 2003; Oswald et al., 2015;
40 Zhang et al., 2009, 2012), and dry deposition is the major HONO loss pathway at night,
41 especially over wet surfaces (He et al., 2006; VandenBoer et al., 2015). However, HONO
42 sources in the planetary boundary layer (PBL) are numerous. HONO is directly emitted from
43 combustion processes, such as automobile emissions (Li et al., 2008b) and biomass burning
44 (Burling et al., 2010; Trentmann et al., 2003). Soil emission via nitrification or denitrification
45 is another source of HONO, which might be important in agriculture region (Maljanen et al.,
46 2013; Oswald et al., 2013; Su et al., 2011). Due to the relatively short photolytic lifetime of
47 HONO, in the order of 10 min around summer noontime, the impacts of the direct emission
48 on HONO distribution and chemistry is highly localized and limited to the source region.

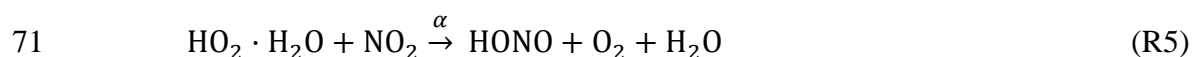
49 HONO is a unique species that is produced through heterogeneous reactions of
50 different precursors, such as NO₂ and HNO₃, on surfaces (R2 - R3):



53 Heterogeneous reactions of NO₂ with organics (R2) on the surfaces have been found to be
54 greatly accelerated by sunlight through photosensitization (George et al., 2005; Kleffmann,

55 2007; Stemmler et al., 2006, 2007) and these reactions on ground surfaces are likely the major
56 daytime HONO source in urban environments (Acker et al., 2006; Villena et al., 2011; Wong
57 et al., 2011). Laboratory studies have confirmed that HNO₃ undergoes photolysis in sunlight
58 at rates 2 - 3 orders of magnitude greater on the surface than in the gas phase (Baergen and
59 Donaldson, 2013; Du and Zhu, 2011; Ye et al., 2016a, b; Zhou et al., 2003; Zhu et al., 2008),
60 producing NO_x and HONO. In low-NO_x environments, photolysis of nitric acid/nitrate
61 deposited on the surface has been proposed to be the major daytime HONO source near the
62 ground surface (Ye et al., 2016b; Zhou et al., 2003, 2011).

63 Several processes within an air mass may lead to volume, or *in situ*, production of
64 HONO. The OH+NO reaction (R-1) in the gas phase may be a significant HONO source in
65 high NO_x and photochemically reactive atmospheres (Kleffmann, 2007; Neuman et al., 2016;
66 Villena et al., 2011), but becomes negligible in low-NO_x environments (Li et al., 2014; Ye et
67 al., 2016b). Two additional gas-phase reactions have been proposed to produce HONO within
68 the air column: between excited NO₂ (NO₂^{*}) and water vapor (R4) (Li et al., 2008a), and
69 between NO₂ and the hydroperoxyl-water complex (HO₂·H₂O) (R5) (Li et al., 2014):



72 However, further laboratory evidence suggests that reaction (R4) is too slow to be important
73 (Carr et al., 2009; Wong et al., 2011). And recent airborne observations have demonstrated
74 that the HONO yield (α) from reaction (R5) is less than 0.03 (Ye et al., 2015). Heterogeneous
75 reactions of NO₂ (R2) on aerosol surfaces and photolysis of particulate nitrate (pNO₃)
76 associated with aerosol particles similar to (R3) also contribute *in situ* HONO production in
77 the air column.

78 Most HONO measurements have been made at ground stations. The observed HONO
79 concentrations reported in the literature represent the HONO levels in the lower PBL under
80 the significant but varying influence of ground surface processes. Thus, it is difficult to
81 distinguish the ground surface HONO sources from the *in situ* HONO sources. Measurements
82 of vertical HONO concentration profiles and HONO fluxes have suggested that ground
83 surfaces can be major HONO sources for the overlying atmosphere in many cases (He et al.,
84 2006; Kleffmann et al., 2003; Stutz et al., 2002; Zhou et al., 2011; VandenBoer et al., 2013;
85 Young et al., 2012), but not in some other cases (Villena et al., 2011). A recent HONO flux
86 measurement has suggested that the HONO source from the forest canopy contributed ~ 60%
87 of the measured HONO budget at the measurement height of 11 m above the forest canopy,

88 and the *in situ* HONO production contributed the remaining ~ 40% (Zhou et al., 2011).
89 Similarly, observational and modeling studies implied a presence of a volume HONO source
90 at 130-m altitude above Houston, TX (Wong et al., 2012, 2013). The relative importance of *in*
91 *situ* HONO production would be expected to increase with altitude due to decreasing
92 influence of the ground surface, at least during the day. Airborne measurements in the air
93 mass above the altitude influenced directly by ground HONO sources should provide more
94 direct and quantitative evidence for *in situ* HONO production in the troposphere. Indeed, the
95 limited number of airborne measurements available have shown that HONO exists not only in
96 substantial amounts in combustion and urban plumes (Neuman et al., 2016) but also
97 throughout the troposphere (Li et al., 2014; Ye et al., 2015; Zhang et al., 2009).

98 Here we report airborne HONO measurement results and findings from five research
99 flights in the Southeast U.S. during the NOMADSS (Nitrogen, Oxidants, Mercury and
100 Aerosol Distributions, Sources and Sinks) 2013 summer field campaign aboard the
101 NSF/NCAR C-130 research aircraft.

102 **2 Experimental**

103 NOMADSS was an airborne field study under the “umbrella” of SAS (Southeast
104 Atmosphere Study). It consisted of nineteen research flights on board the NSF/NCAR C-130
105 aircraft from June 1, 2013 to July 15, 2013. Parameters observed included HONO, HNO₃,
106 particulate nitrate, NO_x, O₃, BrO, OH radicals, HO₂ radicals, RO₂ radicals, aerosol surface
107 area densities (size <1 μm), VOCs, photolysis frequencies, and other meteorology parameters.
108 Table 1 summarizes the instrumentation, time resolution, detection limit, accuracy, and
109 references for the measurements. The results from five out of nineteen flights are presented
110 here to discuss vertical HONO distribution and HONO chemistry in the Southeast U.S. The
111 flight tracks are shown in Figure 1.

112 **2.1 LPAP measurements of HONO and pNO₃**

113 HONO was measured by two long-path absorption photometric (LPAP) systems based
114 on the Griess-Saltzman reaction (Zhang et al., 2012; Ye et al., 2016b). Briefly, ambient air
115 was first brought into the aircraft through a heated PFA inlet, with a residence time of 0.14 s.
116 HONO was scrubbed using de-ionized (DI) water in two 10-turn glass coil samplers and the
117 collected nitrite was then derivatized with 5 mM sulfanilamide (SA) and 0.5 mM N-(1-
118 Naphthyl)-ethylene-diamine (NED) in 40 mM HCl, to form an azo dye. The azo dye was then

119 detected by light absorption at 540 nm using an 4-channel optic fiber spectrometer (LEDSpec,
120 WPI) with two 1-m liquid waveguide capillary flow cells (WPI). Each LPAP system ran a 30-
121 min measurement and zero cycle, with 20 min sampling ambient air and 10 min sampling
122 “zero-HONO” air for baseline correction, and with a 15-min time offset between the two
123 sampling cycles. The combination of the data from the two systems provides continues
124 HONO concentration measurement. The “zero-HONO” air was generated by directing the
125 sample stream through a Na₂CO₃-coated denuder to remove HONO while allowing most of
126 interfering species (NO_x, PAN, and particulate nitrite) to pass through . The absorbance
127 signals were sampled at a rate of 1 Hz, and were averaged into 1-min or 3-min data for
128 analysis.

129 Interference from NO_x, PAN, and particulate nitrite was corrected by subtracting the
130 baseline from the ambient air signal. Due to the low collecting efficiency of these interfering
131 species in the sampling coil and their low concentrations, the combined interference was
132 estimated to be less than 10% of the total signal. Potential interference from peroxyacetic acid
133 (HO₂NO₂) was suppressed by heating the PFA sampling line to 50 °C. The HO₂NO₂ steady
134 state concentration ([HO₂NO₂]_{SS}) was estimated to be less than 1 pptv at temperatures of 20 -
135 30 °C in the background PBL (Gierczak et al., 2005), and thus interference from HO₂NO₂ was
136 negligible. Whereas in power plant and urban plumes in the PBL or biomass burning plumes
137 in the upper free troposphere (FT), HO₂NO₂ interference was not negligible and thus a
138 correction for HONO measurement was made. An upper-limit HO₂NO₂ response efficiency
139 was estimated to be 0.2 for our HONO measurement systems. The estimation was made from
140 the lowest ratio of the measured HONO to the corresponding [HO₂NO₂]_{SS} in cold air masses
141 at high altitude, assuming no HONO existed. HONO concentration were then corrected by
142 subtracting a term of “0.2 × [HO₂NO₂]_{SS}”. The correction was below 10% of the measured
143 HONO concentrations in the PBL plumes. However, there may be over-corrections in the cold
144 free troposphere.

145 The lower detection limit of LPAP-HONO measurement was estimated to be ≤1 pptv,
146 based on 3 times the standard deviation of the zero air signal (N >10). An overall uncertainty
147 of ±(1 + 0.2 [HONO]) pptv was estimated, combining the uncertainties in signal acquisition
148 and processing, air and liquid flow rates, standard preparation, and baseline correction. The
149 accuracy of HONO measurements was confirmed by comparison with a limb-scanning
150 differential optical absorption spectroscopy (DOAS) (Platt and Stutz, 2008) during the
151 NOMADSS 2013 summer field study onboard the C-130 aircraft (Ye et al., 2016b). When

152 measuring in wide power plant plumes where HONO mixing ratios exceeded the lower
153 detection limits of both instruments, the agreement between these two instruments was very
154 good, within the assessed uncertainties (Ye et al., 2016b).

155 Particulate nitrate ($p\text{NO}_3$) was quantitatively collected with a frit disc sampler after a
156 NaCl-coated denuder to remove HNO_3 (Huang et al., 2002). The collected nitrate was reduced
157 to nitrite by a Cd column, and determined using a LPAP system (Zhang et al., 2012). “Zero-
158 $p\text{NO}_3$ ” air was generated to establish measurement baselines for $p\text{NO}_3$ by passing the ambient
159 air through a Teflon filter to remove aerosol particles and then a NaCl-coated denuder to
160 remove HNO_3 before reaching the sampling unit of LPAP. Potential interferences from
161 HONO, NO_x and PAN were corrected by subtracting the baselines from the ambient air
162 signals. The lower detection limit of $p\text{NO}_3$ was estimated to be 2 pptv, based on 3 times the
163 standard deviation of the zero-air signal ($N > 10$). An overall uncertainty of $\pm(2 + 0.3 [p\text{NO}_3])$
164 pptv was estimated.

165 Noisy baselines were observed when the C-130 was flying in the clouds, due to the
166 sampling of cloud droplets by our sampling systems. Because of the lack of a valid way to
167 correct for this interference, all in-cloud measurement data of HONO and $p\text{NO}_3$ have been
168 excluded from the data analysis. In addition, large baseline shifts were observed sometimes
169 when the flow state of the scrubbing solution was disturbed by rapid pressure changes during
170 aircraft’s rapid ascending to or descending from high altitudes. The data were excluded from
171 analysis if the baseline shifts caused by rapid pressure changes could not be reasonably
172 corrected, regardless of the sign or magnitude of the data.

173 **2.2 Supporting measurements**

174 The mixing ratios of a large number of non-methane organic compounds (NMOCs) were
175 measured by Trace Organic Gas Analyzer (TOGA) (Hornbrook et al., 2011a) and Proton-
176 transfer-reaction mass spectrometry (PTR-MS) (Karl et al., 2003; de Gouw and Warneke,
177 2007). The surface area density of fine particles was obtained by the measurement of a
178 Scanning Mobility Particle Sizer (SMPS), under the assumption of preface sphere of aerosol
179 particle. The photolysis frequencies were determined by a Charged-coupled device Actinic
180 Flux Spectroradiometer instrument (CAFS) (Shetter et al., 2002). The mixing ratios of HO_x
181 and RO_2 radicals were measured by a method based on selected-ion chemical-ionization mass
182 spectrometry (SICIMS) (Hornbrook et al., 2011b; Mauldin et al., 2010). The mixing ratios of

183 ozone and NO_x were measured by chemiluminescence instruments (Ridley et al., 2004).
184 Meteorology parameters were provided by state parameter measurements on board the C-130.

185 **3 Results and Discussion**

186 **3.1 General data description**

187 Figure 2 shows the time series of HONO, NO_x , pNO_3 concentrations and the measurement
188 altitude for five selected research flights in the Southeast U.S. during the NOMADSS 2013
189 summer field study. Research flight (RF) #4, RF #5 and RF #17 are race track flights in the
190 background terrestrial areas designed to establish HONO distribution and explore HONO
191 chemistry in background air masses. RF #11 is a race track flight designed to intercept plumes
192 from local power plants and urban areas and explore HONO chemistry therein. All four flights
193 were conducted in the daytime, roughly from 14:00 to 22:00 UTC (10:00 to 18:00 EDT). RF
194 #18 is a race track flight conducted from 20:30 on July 12th to 03:30 on July 13th UTC (16:30
195 to 23:30 on July 12th, 2013 EDT), aiming to study the potential night-time HONO
196 accumulation both in the PBL and the FT.

197 Table 2 summarizes the data statistics for HONO, NO_x and pNO_3 measurements in the
198 PBL and the FT, and Figure 3 shows composite vertical distributions of HONO, NO_x and
199 pNO_3 concentrations from the five flights in the Southeast U.S. during the NOMADSS 2013
200 summer field study. HONO, NO_x and pNO_3 concentrations show horizontal gradients in every
201 race track flight and vary in different race track flights, reflecting the inhomogeneity of air
202 masses in the region. However, there was no significant vertical gradient in HONO, NO_x and
203 pNO_3 concentrations, which will be further discussed below. Except in a few power plant
204 plumes and urban plumes mostly encountered in RF #11, most of the data is representative of
205 background terrestrial air masses. The range of the mixing ratio of HONO is 3.1 – 34.4 pptv.
206 The mean ($\pm 1\text{SD}$) and median values of HONO concentration are 5.6 (± 3.4) pptv and 4.2
207 pptv in the FT, and 11.2 (± 4.3) pptv and 10.3 pptv in the PBL. HONO levels at ~ 4 pptv are
208 typically found in the background FT, but high HONO concentrations up to 15.2 pptv are also
209 observed in the elevated biomass burning plumes. HONO levels at ~ 11 pptv are
210 representative of background conditions in the PBL. High HONO levels up to 34.4 pptv are
211 observed in the power plant plumes and urban plumes in RF #11 (see section 3.4) and RF #
212 17. These measured HONO values are consistent with the range of 4 – 74 pptv in the
213 troposphere over Northern Michigan (Zhang et al., 2009), but are significantly lower than 100
214 - 150 pptv in the morning residual layer over an industrial region of Northern Italy (Li et al.,

215 2014), where the levels of HONO precursors, such as NO_x and pNO_3 , were much higher. The
216 HONO concentrations were also consistent with the levels reported for the same region during
217 the Southeast Nexus Experiment on the NOAA WP-3D aircraft (Neuman et al., 2016), that is,
218 “indistinguishable from zero within the 15 parts per trillion by volume measurement
219 uncertainty” in the background air and up to 150 pptv in the power plant plumes during the
220 day. The lower HONO concentrations measured in the power plant plumes in this study than
221 the daytime values reported by Neuman et al (2016) probably reflects greater dilution of
222 smaller plumes encountered by the C-130 than by the WP-3D, as indicated by much lower
223 NO_x levels observed, up to 1.8 ppbv vs up to 60 ppbv.

224 The range of the mixing ratio of NO_x is from several pptv to around 1.8 ppbv. The
225 mean ($\pm 1\text{SD}$) and median values of NO_x concentration are 94 (± 53) pptv and 92 pptv in the
226 FT, and 316 (± 182) pptv and 279 pptv in the PBL. The mixing ratios of NO_x are mostly
227 between 50 - 150 pptv in the background conditions in the FT and between 200 - 500 pptv in
228 the background conditions in the PBL. Similar to HONO, high values of NO_x also occur in the
229 urban and power plant plumes in the PBL (up to 1.8 ppbv) and in the biomass burning plumes
230 in the FT (up to 0.6 ppbv).

231 Fewer measurement data points are available for pNO_3 , compared to those for NO_x
232 and HONO, due to air bubble formation in the flow cell of the pNO_3 system, especially at
233 high altitudes. The range of the mixing ratio of pNO_3 is from 3 pptv to 186 pptv, with the
234 mean ($\pm 1\text{SD}$) and median values of 35 (± 39) pptv and 15 pptv in the FT, and 76 (± 45)
235 pptv and 66 pptv in the PBL. The pNO_3 levels were highly variable in both the FT and the
236 PBL. In the FT, the pNO_3 levels were often under 10 pptv, but high concentrations up to 179
237 pptv were also observed in elevated biomass burning plumes. In the PBL, high pNO_3 levels
238 were sometimes observed in relative clean conditions; whereas, low pNO_3 levels were
239 observed in high HONO and NO_x power plant plumes. Both the N(V) level ($= [\text{HNO}_3] +$
240 $[\text{pNO}_3]$) and the partitioning between HNO_3 and pNO_3 seem to play roles in determining the
241 pNO_3 level.

242 **3.2 HONO contribution from ground-level sources**

243 There are several ground-level HONO sources that may contribute to the HONO
244 budget in the overlying atmosphere. They include anthropogenic sources, such as power plant
245 and automobile emissions (Li et al., 2008b; Neuman et al., 2016), and natural processes, such
246 as soil emission (Maljanen et al., 2013; Oswald et al., 2013; Su et al., 2011), heterogeneous

247 reactions of NO₂ (Acker et al., 2006; George et al., 2005; Ndour et al., 2008, 2009; Ramazan
 248 et al., 2006) and surface HNO₃ photolysis (Ye et al., 2016b; Zhou et al., 2003,2011). Since
 249 HONO photolytic lifetime is relatively short, e.g. 8 - 16 min in RF #4, RF #5, RF #11 and RF
 250 #17, a steep negative vertical gradient of HONO concentration would be expected if a
 251 significant contribution originated from the ground. The lack of a significant vertical gradient
 252 in the measured HONO concentrations (Fig. 3a) thus suggests that the ground contribution is
 253 either limited to the shallow layer of the boundary layer near the ground, below the C-130
 254 lowest flight altitude of 300 m, or small relative to the *in situ* production of HONO in the air
 255 column (Ye et al., 2017).

256 To further examine the potential HONO contribution from the ground sources, vertical
 257 profiles of HONO, NO_x, and pNO₃, are compared with those of potential temperature (K) and
 258 isoprene measured, for example, in the first race-track of RF#4 from 11:00 – 12:15 LT (Fig.
 259 4). The PBL height (*H*) was ~ 1200 m as indicated by the constant potential temperature (Fig.
 260 4e). The vertical distribution of isoprene originating from the ground can be expressed with
 261 the following equation (Eq.1):

$$262 \quad \ln\left(\frac{C}{C_0}\right) = -\frac{k\tau}{H}h = -\frac{h}{h^*} \quad (\text{Eq. 1})$$

263 where *C*₀ and *C* are its concentrations near the ground and at the altitude *h*, *k* is the pseudo-
 264 first order degradation rate constant, *τ* is the average mixing time in the PBL, and *h** (= *H*/(*kτ*))
 265 is its characteristic transport height within one degradation lifetime of isoprene.

266 According to the best fit of (Eq.1) to the observed isoprene data (Fig. 4d), its characteristic
 267 transport height *h** is estimated 692 m for isoprene. Assuming isoprene is mainly oxidized by
 268 the OH radical whose average concentration was found to be ~ 3 × 10⁶ mole cm⁻³ in the PBL
 269 in the Southeast U.S. during the NOMADSS study (Kaser et al., 2015), the pseudo-first order
 270 degradation rate constant of ~ 3.0 × 10⁻⁴ s⁻¹ (or the degradation rate of ~ 0.93 h⁻¹) is
 271 determined for isoprene. Based on a boundary layer height of ~1.2 km (Fig. 4e), an average
 272 PBL mixing time *τ* is estimated to be ~1.6 h between 11:00 – 12:15 LT of RF #4. With a
 273 photolytic lifetime of ~ 11 min for HONO, about 11% of the HONO originated from the
 274 ground level is expected to reach the altitude of 300 m, the lowest flight altitude of the C-130
 275 aircraft between 11:00 – 12:15 LT in RF #4. The vertical mixing of the PBL is enhanced from
 276 the morning to the afternoon, as the ground surface is heated by solar radiation gradually
 277 during the day. The average mixing time in the PBL is reduced from ~ 3 h in the morning, to
 278 ~ 1.5 h around noontime, and to ~ 30 min in the afternoon, determined from isoprene
 279 gradients from RF #4, #5 and #17. About 50% of the ground emitted HONO could survive

280 and be transported to lower measurement altitudes. Again, if this ground source contribution
281 was significant, the HONO concentration profile should exhibit a significant gradient,
282 probably more pronounced than that of isoprene due to its shorter lifetime. The lack of such a
283 vertical HONO gradient in the measured HONO concentration profiles (Fig. 3a) suggests that
284 the contribution from ground HONO sources to the observed HONO concentrations in the
285 PBL above 300 m is insignificant.

286 The NO_x level was ≤ 0.5 ppbv in the PBL over the Southeast U.S. (Figure 2),
287 excluding the power plant plumes. Based on an upper limit HONO/ NO_x ratio of 0.05 for
288 urban atmosphere at ground level (Villena et al., 2011), the initial HONO concentration would
289 be ≤ 25 pptv in the source air mass on the ground level. With a transport time of ≥ 0.5 h,
290 i.e., ≥ 3 times of the HONO photolysis lifetime, the contribution from the ground HONO
291 source would be ≤ 1 pptv. This analysis supports the conclusion that contribution of surface
292 HONO source to the PBL HONO budget is insignificant.

293 3.3 Daytime HONO chemistry in low NO_x areas

294 After removing the data measured in the urban and power plant plumes, the daytime HONO
295 concentrations are within the range of 5 - 15 pptv throughout the PBL in the background
296 terrestrial areas in the five race-track research flights. Photolysis is the dominant sink for
297 HONO, with a photolysis lifetime of 8 - 16 min during these four daytime flights (RF #4, RF
298 #5, RF #11, and RF #17). Therefore, there must be a significant volume HONO source, up to
299 173 pptv h^{-1} , within the air mass to sustain the observed HONO concentrations.

300 Both NO_x and pNO_3 are potential HONO precursors in the air column. While HONO
301 correlates moderately with NO_x ($r^2 = 0.45$, Fig S1), it only weakly correlates with pNO_3 ($R^2 =$
302 0.17). It appears at first that NO_x is a more important HONO precursor than pNO_3 . However,
303 the detailed analysis below suggests that NO_x is only a minor precursor to the observed
304 HONO, and photolysis of pNO_3 is the major *in situ* HONO source.

305 The upper limit of photo-stationary state HONO concentration ($[\text{HONO}]_{\text{pss}}$) was
306 calculated using Equation 2 that takes into account all the known HONO source contributions
307 from NO_x -related reactions, including gaseous reactions of OH and NO (R-1), excited NO_2
308 (NO_2^*) and water vapor (R4) (Carr et al., 2009; Li et al., 2008a), NO_2 and the hydroperoxyl-
309 water complex ($\text{HO}_2 \cdot \text{H}_2\text{O}$) with an upper limit HONO yield of 3% (R5a)(Li et al., 2014; Ye et
310 al., 2015), and heterogeneous reaction of NO_2 on aerosol surfaces (R2) using an upper limit

311 uptake coefficient of 10^{-4} reported in the literature (George et al., 2005; Monge et al., 2010;
 312 Ndour et al., 2008, 2009; Stemmler et al., 2006, 2007):

$$313 \quad [\text{HONO}]_{pss} = \frac{k_{-1}[\text{NO}][\text{OH}] + k_4[\text{NO}_2^*][\text{H}_2\text{O}] + \alpha k_5[\text{NO}_2][\text{HO}_2 \cdot \text{H}_2\text{O}] + k_2 S_{aerosol}[\text{NO}_2]}{J_{\text{HONO}} + k_{\text{OH}} - \text{HONO}[\text{OH}]} \quad (\text{Eq. 2})$$

314 where $S_{aerosol}$ is the aerosol surface area density. It should be noted that the upper limit values
 315 of rate constants were used in the calculation to avoid the underestimation of $[\text{HONO}]_{pss}$
 316 value. Under typical daytime conditions in the PBL with the median measured values of
 317 reactants, the upper limit $[\text{HONO}]_{pss}$ value is less than 2 pptv, much lower than the median
 318 measured HONO concentration of ~ 11 pptv. Figure 5a shows the relationship ($r^2 = 0.40$)
 319 between the photolytic HONO loss rate with the sum of HONO production rates from all the
 320 NO_x -related reactions calculated with upper-limit reaction rate constants. A slope of about
 321 0.19 indicates that the contribution from these NO_x -related reactions to the volume HONO
 322 source is minor in the background troposphere, despite the good correlation between HONO
 323 and NO_x .

324 Photolysis of HNO_3 on surfaces has been found to proceed at a much higher rate than
 325 in the gas phase (Baergen and Donaldson, 2013; Du and Zhu, 2011; Ramazan et al., 2004; Ye
 326 et al., 2016b; Zhou et al., 2003; Zhu et al., 2008), with HONO as the major product on
 327 environmental surfaces (Ye et al., 2016a, 2017). Furthermore, photolysis of particulate nitrate
 328 has been found to be the major daytime HONO source in the marine boundary layer (Ye et al.,
 329 2016b). To examine the role of particulate nitrate as a potential HONO source in the
 330 troposphere, aerosol samples were collected and used in the light-exposure experiments to
 331 determine the photolysis rate constants for particulate nitrate in the laboratory. The
 332 determined pNO_3 photolysis rate constant ($J_{\text{pNO}_3}^N$) varies over a wide range, from $8.3 \times 10^{-5} \text{ s}^{-1}$
 333 to $3.1 \times 10^{-4} \text{ s}^{-1}$, with a median of $2.0 \times 10^{-4} \text{ s}^{-1}$ and a mean ($\pm 1 \text{ SD}$) of $1.9 (\pm 1.2) \times 10^{-4} \text{ s}^{-1}$,
 334 when normalized to tropical noontime conditions at ground level (solar zenith angle = 0°),
 335 and the average HONO to NO_2 relative yield is 2.0 (Ye et al., 2017). Figure 6b shows the
 336 relationship between the photolytic HONO loss rate ($J_{\text{HONO}} \times [\text{HONO}]$) and the volume HONO
 337 production rates from pNO_3 photolysis ($2/3 \times J_{\text{HNO}_3} \times [\text{pNO}_3]$). The median $J_{\text{pNO}_3}^N$ of $\sim 2.0 \times$
 338 10^{-4} s^{-1} was used to calculate the ambient J_{pNO_3} by scaling to J_{HNO_3} :

$$339 \quad J_{\text{pNO}_3} = J_{\text{pNO}_3}^N \times \frac{J_{\text{HNO}_3}}{7.0 \times 10^{-7} \text{ s}^{-1}} \quad (\text{Eq. 3}),$$

340 where J_{HNO_3} is the photolysis rate constant of gas-phase HNO_3 calculated from light intensity
 341 measurement on the C-130 aircraft, and $7.0 \times 10^{-7} \text{ s}^{-1}$ is the photolysis rate constant of gas-
 342 phase HNO_3 under the tropical noontime condition at ground level (solar zenith angle = 0°). A

343 slope of 0.69 can be derived from Figure 5b, suggesting that pNO₃ photolysis is the major
344 volume HONO source. However, the r² of 0.34 is not as strong as expected from pNO₃
345 photolysis being the major volume HONO source. It may be in part due to the use of a single
346 median $J_{pNO_3}^N$ value of $\sim 2.0 \times 10^{-4} \text{ s}^{-1}$ in the calculations of the ambient J_{pNO_3} and the
347 production rates of HONO in Figure 5b; the actual $J_{pNO_3}^N$ values are highly variable, ranging
348 from $8.3 \times 10^{-5} \text{ s}^{-1}$ to $3.1 \times 10^{-4} \text{ s}^{-1}$ (Ye et al., 2017). HONO source contribution from
349 particulate nitrate photolysis in Figure 5b are thus estimates of the *in situ* HONO production
350 rates from pNO₃ photolysis in different air masses.

351 HONO photolysis has been found to be an important or even a major OH primary
352 source in the atmosphere near the ground surface (Elshorbany et al., 2010; He et al., 2006;
353 Kleffmann et al., 2003; Villena et al., 2011; Zhou et al., 2011). However, HONO is not a
354 significant daytime OH precursor in the background troposphere away from the ground
355 surface. Based on the measurement results in this study, the mean (\pm SD) contribution of
356 HONO photolysis to the OH source budget is 53 (\pm 21) pptv h⁻¹ in the PBL and 44 (\pm 26) pptv
357 h⁻¹ in the FT (Table S1), respectively, less than 10% of the OH production contributed by O₃
358 photolysis. Since HONO is mainly produced from photolysis of particulate nitrate, it becomes
359 an important intermediate product of a photochemical renoxification process recycling nitric
360 acid and nitrate back to NO_x. The regenerating rate of NO_x of about 38 (\pm 23) pptv h⁻¹ via
361 pNO₃ photolysis (Table S1) is equivalent to an air column NO_x source of $\sim 2.3 \times 10^{-6} \text{ mol m}^{-2}$
362 h⁻¹ in the 1.5- km PBL, a considerable supplementary NO_x source in the low-NO_x background
363 area.

364 It should be pointed out that particulate nitrate is in a dynamic equilibrium with gas-
365 phase HNO₃, the later accounts for a larger (or even dominant) fraction of total nitrate
366 (pNO₃+HNO₃) and is photochemically inert. The overall photolysis of pNO₃+HNO₃ would be
367 much slower than indicated by J_{pNO_3} . In addition, oxidation of NO_x via several reactions will
368 replenish the pNO₃+HNO₃ reservoir. The results reported here and in earlier papers (Reed et
369 al., 2017; Ye et al., 2016a) suggest that there is a rapid cycling in reactive nitrogen species in
370 the low-NO_x atmosphere, sustaining the observed levels of HONO and pNO₃.

371 **3.4 HONO chemistry in plumes**

372 One of the objectives of RF #11 was to study the chemistry of HONO in urban and coal fired
373 power plant plumes. The arrows and corresponding labels in Figure 2 indicate the urban
374 plumes (U1-U3) and power plant plumes (P1-P4). CO and benzene were used to identify

375 influence from urban plumes, SO₂ to identify influence from power plant plumes, and
376 acetonitrile to identify the influence of biomass burning plumes (Fig. S2). The plumes U1-U3
377 were identified as urban plumes from cities of Birmingham (U1, U3) and Montgomery (U2)
378 in Alabama, respectively, and plumes P1-P4 were identified as power plant plumes from
379 power plants in Monroe county (P1-P3) and Putman county(P4) in Georgia, respectively. The
380 influence of biomass burning plumes was negligible as acetonitrile concentration was low and
381 stable. The power plant plumes were generated from high-intensity point sources, and thus
382 had features of narrow but high peaks of both HONO and NO_x concentrations in the time-
383 series plots (Figs. 2, 6 & S2). In contrast, the urban plumes were generated from area sources
384 and thus were shown as broad peaks of HONO and NO_x in the time-series plot with low levels
385 of NO_x (mostly below 500 pptv) (Figs. 2, 6 & S2). There were a few sharp but small NO_x
386 peaks within the broad urban plumes, reflecting the contributions of some point sources in the
387 urban areas. The observed HONO/NO_x ratio was 0.019 (± 0.004) in the power plant plumes
388 (e.g., P4) and 0.057 (± 0.0019) in urban plumes, significantly higher than the typical
389 HONO/NO_x emission ratio of ~0.002 in the fresh power plant plumes (Neuman et al., 2016)
390 and ≤0.01 in automobile exhaust (Kurtenbach et al., 2001; Li et al., 2008b). The elevated
391 HONO/NO_x ratios observed in the plumes suggest that the observed HONO was mostly
392 produced from precursors within the air mass during the transport. Based on the distances
393 between measurement locations from the power plants or the centres of urban areas and wind
394 speed, the transport times of these plumes were estimated to be ≥ 1 h, ~ 5 times longer than
395 HONO photolysis lifetime of 8 - 16 min, again suggesting that most of the observed HONO in
396 the plumes was produced *in situ* within the air masses.

397 Figure 6 shows the time-series plot of HONO budgets within the air masses sampled
398 by the C-130 aircraft during flight RF# 11, comparing its photolysis loss rate with its
399 production rates from pNO₃ photolysis and from all the NO_x-related reactions combined.
400 Photolysis of particulate nitrate appears to be the major volume HONO source in all urban
401 plumes and in most of the power plant plumes except for plume P4 observed here. NO_x was
402 generally more important as a HONO precursor in the power plant plumes than in the urban
403 plumes and in low-NO_x background air masses, due to higher levels of NO_x (up to 1.8 ppb in
404 Figs. 2c and S2), OH radical and aerosol surface density. For example, all the NO_x-related
405 reactions combined contributed up to 52% of the total volume HONO source required to
406 sustain the observed HONO concentration in plume P4 (Fig. 6). In fresh and larger power
407 plant plumes encountered during the RF #7 to Ohio River Valley (X. Zhou, unpublished data),

408 over 20 ppb NO_x was detected, and the NO_x-related reactions, mainly the NO+OH reaction,
409 were found to account for almost all the required HONO source strength to sustain the
410 observed HONO, in agreement with Neuman et al. (2016). The power plant plumes undergo
411 rapid physical and photochemical evolution during the day, such as dilution and NO_x-to-
412 HNO₃ conversion. Thus, the relative contributions from NO_x-related reactions and particulate
413 nitrate photolysis as HONO sources change rapidly as the plumes age.

414 **3.5 Night-time HONO chemistry**

415 Nighttime HONO accumulation has been widely observed at the ground level (Kleffmann et
416 al., 2003; Oswald et al., 2015; 2008; Stutz et al., 2002, 2010; VandenBoer et al., 2013, 2014,
417 2015), contributed by various anthropogenic and natural HONO sources on the ground. The
418 main objective of RF #18 was to study the night-time HONO evolution in both the nocturnal
419 residual layer and the nocturnal FT. After sunset, the surface cooling promotes the formations
420 of a inversion layer near the ground surface and a nocturnal residual layer above; the
421 contribution from ground HONO sources then becomes negligible to the air masses beyond
422 the surface inversion layer. Meanwhile, no effective HONO sinks, such as photolysis,
423 oxidation by OH and dry deposition, exist in the nocturnal residual layer. Thus the HONO
424 accumulation, if any, is a net contribution from dark heterogeneous NO₂ reaction on aerosol
425 surfaces (R2).

426 The C-130 flew in an elongated race track pattern along a north-south direction, about
427 140 km from Nashville, TN (Fig. 1), alternating between the PBL (1200 m) and the FT (2500
428 m), from late afternoon to midnight local time (Fig. 2). In the FT, HONO and NO_x
429 concentrations were relatively stable throughout the afternoon and the night, staying around 4
430 ppt and 90 pptv respectively. The lack of night-time HONO accumulation is expected from
431 the low levels of HONO precursors, mostly NO₂, and surface area of aerosol particles in the
432 FT (Fig. 2).

433 The conditions in the PBL were far more variable and complicated. There were strong
434 horizontal gradients of NO_x, pNO₃ and HONO in the PBL, with higher concentrations at the
435 southern end and lower concentrations at the northern end of the flight track. Back-trajectory
436 analysis using NOAA's HYSPLIT model (Stein et al., 2015) indicates that the encountered air
437 masses in the PBL at the southern end passed over Nashville, about 140 km northeast of the
438 sample area, with a transport time of about 6 h (Fig. S3a), while the air masses at the northern
439 end stayed to north of Nashville (Fig. S3b). Therefore, the anthropogenic emissions from the

440 metropolitan area of Nashville contributed to the higher concentrations of pollutants observed
 441 at the southern end of the flight track. There were also trends of increasing concentrations of
 442 NO_x, pNO₃ and HONO with time after the sunset (Fig. 2). This was probably a result of less
 443 dispersion and dilution of anthropogenic pollutants, including NO_x, as the PBL became more
 444 stable after sunset. Furthermore, as time progressed from late afternoon into evening and
 445 night, the air masses were less photochemically aged during the transport from the source
 446 areas, due to the decreasing solar light intensity and shorter solar light exposure time.

447 Because of the large spatial and temporal variations in the concentrations of HONO and
 448 its precursors in the PLB (Fig. 2), it is difficult to directly evaluate the nighttime HONO
 449 accumulation from HONO measurements alone. The concentration ratio of HONO and its
 450 dominant nighttime precursor, NO₂, can be used as an indicator of nighttime HONO
 451 accumulation. As the air masses at measurement altitude of 1200 m decoupled from the
 452 ground-level processes after sunset, the HONO production ($P(\text{HONO})$) from heterogeneous
 453 NO₂ reaction (R2) on aerosol surface becomes the only HONO source, and can be expressed
 454 by the following equations (Eq. 4 and Eq. 5):

$$455 \quad P(\text{HONO}) = \frac{1}{4} \times \left[\frac{s}{v} \right] \times \sqrt{\frac{8RT}{\pi M}} \times \gamma \times [\text{NO}_2] \quad (\text{Eq.4})$$

$$456 \quad \frac{P(\text{HONO})}{[\text{NO}_2]} = \frac{1}{4} \times \left[\frac{s}{v} \right] \times \sqrt{\frac{8RT}{\pi M}} \times \gamma \quad (\text{Eq.5})$$

457 where $\left[\frac{s}{v} \right]$ is the specific aerosol surface area density, R is the gas constant, K the absolute
 458 temperature, M the molecular weight of NO₂, and γ is the dark uptake coefficient of NO₂
 459 leading to HONO production. The NO₂-normalized HONO accumulation over time, $\Delta \frac{[\text{HONO}]}{[\text{NO}_2]}$,
 460 can then be calculated by equation (Eq. 6):

$$461 \quad \Delta \frac{[\text{HONO}]}{[\text{NO}_2]} \sim \frac{1}{4} \times \left[\frac{s}{v} \right] \times \sqrt{\frac{8RT}{\pi M}} \times \gamma \times \Delta t \quad (\text{Eq. 6})$$

462 Assuming a dark uptake coefficient γ of 1×10^{-5} of NO₂ on aerosol (George et al., 2005;
 463 Monge et al., 2010; Ndour et al., 2008; Stemmler et al., 2006, 2007) with a $\left[\frac{s}{v} \right]$ value of $\sim 10^{-4}$
 464 m⁻¹, a relative HONO accumulation rate, $\Delta \frac{[\text{HONO}]}{[\text{NO}_2]} / \Delta t$ of $\sim 0.0003 \text{ h}^{-1}$ is estimated using the
 465 equation (Eq. 6), equivalent to a HONO accumulation of 0.13 pptv hr⁻¹ at a constant NO₂
 466 concentration of 400 pptv. Such a low HONO accumulation rate is below our measurement
 467 detection limit. Indeed, the calculated HONO to the NO_x ratio using the measurement data
 468 stayed almost unchanged with time (Fig. 7), well within the observational variability after the

469 sunset, suggesting no significant volume production of HONO in the nocturnal boundary
470 layer.

471 **4 Conclusions**

472 Substantial levels of HONO existed during the day in both the PBL (median ~ 11 pptv) and
473 the FT (median ~ 4 pptv) over the Southeast U.S. during the NOMADSS 2013 summer field
474 study. The ground HONO sources did not significantly contribute to the HONO budget in the
475 PBL above the minimum measurement heights of 300 m. HONO budget analysis suggests
476 that photolysis of particulate nitrate was the major volume HONO source (~69%), while the
477 sum of known NO_x-related reactions a minor HONO source (~19%) in the low-NO_x
478 background air masses. HONO was not a significant daytime OH precursor in the PBL away
479 from the ground surface; however, HONO was an important intermediate product of
480 photolysis of particulate nitrate in the renoxification process. Up to several tens pptv of
481 HONO were observed in power plant plumes and urban plumes during the day, mostly
482 produced *in situ* from precursors including NO_x and pNO₃. No significant night-time HONO
483 accumulation was observed in the nocturnal residual layer and the free troposphere, due to
484 low levels of NO_x and specific aerosol surface area.

485

486 **Acknowledgements**

487 This research is funded by National Science Foundation (NSF) grants (AGS-1216166, AGS-
488 1215712, and AGS-1216743). We would like to acknowledge operational, technical, and
489 scientific support provided by NCAR, sponsored by the National Science Foundation. The
490 data are available in our project data archive
491 (http://data.eol.ucar.edu/master_list/?project=SAS). Any opinions, findings, and conclusions
492 or recommendations expressed in this paper are those of the authors and do not necessarily
493 reflect the views of NSF.

494

495 **References**

496 Acker, K., Moller, D., Wieprecht, W., Meixner, F. X., Bohn, B., Gilge, S., Plass-Dulmer, C.,
497 and Berresheim, H.: Strong daytime production of OH from HNO₂ at a rural mountain site,
498 *Geophys. Res. Lett.*, 33, Artn L02809,10.1029/2005gl024643, 2006.

499 Baergen, A. M., and Donaldson, D. J.: Photochemical renoxification of nitric acid on real
500 urban grime, *Environ. Sci. Technol.*, 47, 815-820, 10.1021/es3037862, 2013.

501 Burling, I. R., Yokelson, R. J., Griffith, D. W. T., Johnson, T. J., Veres, P., Roberts, J. M.,
502 Warneke, C., Urbanski, S. P., Reardon, J., Weise, D. R., Hao, W. M., and de Gouw, J.:
503 Laboratory measurements of trace gas emissions from biomass burning of fuel types from
504 the southeastern and southwestern United States, *Atmos. Chem. Phys.*, 10, 11115-11130,
505 2010.

506 Carr, S., Heard, D. E., and Blitz, M. A.: Comment on "Atmospheric hydroxyl radical
507 production from electronically excited NO₂ and H₂O", *Science*, 324, 2009.

508 de Gouw, J., and Warneke, C.: Measurements of volatile organic compounds in the earth's
509 atmosphere using proton-transfer-reaction mass spectrometry, *Mass Spectrom. Rev.*, 26,
510 223-257, 2007.

511 Du, J., and Zhu, L.: Quantification of the absorption cross sections of surface-adsorbed nitric
512 acid in the 335-365 nm region by Brewster angle cavity ring-down spectroscopy, *Chem.*
513 *Phys. Lett.*, 511, 213-218, 10.1016/j.cplett.2011.06.062, 2011.

514 Elshorbany, Y. F., Kleffmann, J., Kurtenbach, R., Lissi, E., Rubio, M., Villena, G., Gramsch,
515 E., Rickard, A. R., Pilling, M. J., and Wiesen, P.: Seasonal dependence of the oxidation
516 capacity of the city of Santiago de Chile, *Atmos. Environ.*, 44, 5383-5394,
517 10.1016/j.atmosenv.2009.08.036, 2010.

518 Finlayson-Pitts, B. J., and J. N. Pitts, Jr.: *Chemistry of the Upper and Lower Atmosphere:*
519 *Theory, Experiments, and Applications*, Academic Press, San Diego, California, 2000.

520 Flagan, R. C.: Electrical mobility methods for sub-micrometer particle characterization. In
521 *Aerosol Measurement: Principles, Techniques, and Applications*, Third Edition (eds P.
522 Kulkarni, P. A. Baron and K. Willeke), pp339-364, John Wiley & Sons, New York, 2002.

523 George, C., Strekowski, R. S., Kleffmann, J., Stemmler, K., and Ammann, M.:
524 Photoenhanced uptake of gaseous NO₂ on solid-organic compounds: a photochemical
525 source of HONO?, *Faraday Discuss.*, 130, 195-210, 2005.

526 Gierczak, T., Jimenez, E., Riffault, V., Burkholder, J. B., and Ravishankara, A. R.: Thermal
527 decomposition of HO₂NO₂ (peroxynitric acid, PNA): Rate coefficient and determination of
528 the enthalpy of formation, *J. Phys. Chem. A*, 109, 586-596, 2005.

529 He, Y., Zhou, X. L., Hou, J., Gao, H. L., and Bertman, S. B.: Importance of dew in controlling
530 the air-surface exchange of HONO in rural forested environments, *Geophys. Res. Lett.*, 33,
531 2006.

532 Hornbrook, R. S., Blake, D. R., Diskin, G. S., Fried, A., Fuelberg, H. E., Meinardi, S.,
533 Mikoviny, T., Richter, D., Sachse, G. W., Vay, S. A., Walega, J., Weibring, P.,
534 Weinheimer, A. J., Wiedinmyer, C., Wisthaler, A., Hills, A., Riemer, D. D., and Apel, E.
535 C.: Observations of nonmethane organic compounds during ARCTAS - Part 1: Biomass
536 burning emissions and plume enhancements, *Atmos. Chem. Phys.*, 11, 11103-11130,
537 2011a.

538 Hornbrook, R. S., Crawford, J. H., Edwards, G. D., Goyea, O., Mauldin, R. L., Olson, J. S.,
539 and Cantrell, C. A.: Measurements of tropospheric HO₂ and RO₂ by oxygen dilution
540 modulation and chemical ionization mass spectrometry, *Atmos. Meas. Tech.*, 4, 735-756,
541 2011b.

542 Huang, G., Zhou, X., Deng, G., Qiao, H., and Civerolo, K.: Measurements of atmospheric
543 nitrous acid and nitric acid, *Atmos. Environ.*, 36, 2225-2235, 2002.

544 Kaser, L., Karl, T., Yuan, B., Mauldin, R. L. III, Cantrell, C. A., Guenther, A. B., Patton, E.
545 G., Weinheimer, A. J., Knote, C., Orlando, J., Emmons, L., Apel, E., Hornbrook, Shertz,
546 R., S., Ullmann, K., Hall, S., Graus, M., de Gouw, J., Zhou, X., and Ye, C.: chemistry-
547 turbulence interactions and mesoscale variability influence the cleansing efficiency of the
548 atmosphere, *Geophys. Res. Lett.*, 42, doi:10.1002/2015GL066641, 2015.

549 Karl, T., Jobson, T., Kuster, W.C., Williams, E., Stutz, J., Shetter, R., Hall, S.R., Goldan, P.,
550 Fehsenfeld, F., and W. Lindinger, W.: The use of Proton-Transfer-Reaction Mass
551 Spectrometry to Characterize VOC Sources at the La Porte Super Site during the Texas Air
552 Quality Study 2000, *J. Geophys. Res.*, 108, doi: 10.1029/2002JD003333, 2003.

553 Kleffmann, J., Kurtenbach, R., Lorzer, J., Wiesen, P., Kalthoff, N., Vogel, B., and Vogel, H.:
554 Measured and simulated vertical profiles of nitrous acid - Part I: Field measurements,
555 *Atmos. Environ.*, 37, 2949-2955, 2003.

556 Kleffmann, J.: Daytime sources of nitrous acid (HONO) in the atmospheric boundary layer,
557 *Chemphyschem*, 8, 1137-1144, 10.1002/cphc.200700016, 2007.

558 Kurtenbach, R., Becker, K. H., Gomes, J. A. G., Kleffmann, J., Lorzer, J. C., Spittler, M.,
559 Wiesen, P., Ackermann, R., Geyer, A., and Platt, U.: Investigations of emissions and
560 heterogeneous formation of HONO in a road traffic tunnel, *Atmos. Environ.*, 35, 3385-
561 3394, Doi 10.1016/S1352-2310(01)00138-8, 2001.

562 Li, S. P., Matthews, J., and Sinha, A.: Atmospheric hydroxyl radical production from
563 electronically excited NO₂ and H₂O, *Science*, 319, 1657-1660, 2008a.

564 Li, X., Rohrer, F., Hofzumahaus, A., Brauers, T., Haseler, R., Bohn, B., Broch, S., Fuchs, H.,
565 Gomm, S., Holland, F., Jager, J., Kaiser, J., Keutsch, F. N., Lohse, I., Lu, K. D., Tillmann,
566 R., Wegener, R., Wolfe, G. M., Mentel, T. F., Kiendler-Scharr, A., and Wahner, A.:
567 Missing gas-phase source of HONO inferred from Zeppelin measurements in the
568 troposphere, *Science*, 344, 292-296, 2014.

569 Li, Y. Q., Schwab, J. J., and Demerjian, K. L.: Fast time response measurements of gaseous
570 nitrous acid using a tunable diode laser absorption spectrometer: HONO emission source
571 from vehicle exhausts, *Geophys. Res. Lett.*, 35, 2008b.

572 Maljanen, M., Yli-Pirila, P., Hytonen, J., Joutsensaari, J., and Martikainen, P. J.: Acidic
573 northern soils as sources of atmospheric nitrous acid (HONO), *Soil. Biol. Biochem.*, 67,
574 94-97, 10.1016/j.soilbio.2013.08.013, 2013.

575 Mauldin, R., Kosciuch, E., Eisele, F., Huey, G., Tanner, D., Sjostedt, S., Blake, D., Chen, G.,
576 Crawford, J., and Davis, D.: South Pole Antarctica observations and modeling results: New
577 insights on HO_x radical and sulfur chemistry, *Atmos. Environ.*, 44, 572-581, 2010.

578 Monge, M. E., D'Anna, B., Mazri, L., Giroir-Fendler, A., Ammann, M., Donaldson, D. J., and
579 George, C.: Light changes the atmospheric reactivity of soot, *P. Natl. Acad. Sci. USA*, 107,
580 6605-6609, 2010.

581 Ndour, M., D'Anna, B., George, C., Ka, O., Balkanski, Y., Kleffmann, J., Stemmler, K., and
582 Ammann, M.: Photoenhanced uptake of NO₂ on mineral dust: Laboratory experiments and
583 model simulations, *Geophys. Res. Lett.*, 35, 2008.

584 Ndour, M., Nicolas, M., D'Anna, B., Ka, O., and George, C.: Photoreactivity of NO₂ on
585 mineral dusts originating from different locations of the Sahara desert, *Phys. Chem. Chem.*
586 *Phys.*, 11, 1312-1319, 2009.

587 Neuman, J.A., Trainer, M., Brown, S.S., Min, K.-E., Nowak, J.B., Parrish, D.D., Peischl, J.,
588 Pollack, I.B., Roberts, J.M., Ryerson, T.B., and Veres, P.R.: HONO emission and
589 production determined from airborne measurements over the Southeast U.S., *J. Geophys.*
590 *Res.-Atmos.*, 121, 9237-9250, 2016.

591 Oswald, R., Behrendt, T., Ermel, M., Wu, D., Su, H., Cheng, Y., Breuninger, C., Moravek,
592 A., Mougou, E., Delon, C., Loubet, B., Pommerening-Roser, A., Sorgel, M., Poschl, U.,
593 Hoffmann, T., Andreae, M. O., Meixner, F. X., and Trebs, I.: HONO emissions from soil
594 bacteria as a major source of atmospheric reactive nitrogen, *Science*, 341, 1233-1235,
595 10.1126/science.1242266, 2013.

596 Oswald, R., Ermel, M., Hens, K., Novelli, A., Ouwersloot, H. G., Paasonen, P., Petaja, T.,
597 Sipila, M., Keronen, P., Back, J., Konigstedt, R., Beygi, Z. H., Fischer, H., Bohn, B.,
598 Kubistin, D., Harder, H., Martinez, M., Williams, J., Hoffmann, T., Trebs, I., and Sorgel,
599 M.: A comparison of HONO budgets for two measurement heights at a field station within
600 the boreal forest in Finland, *Atmos. Chem. Phys.*, 15, 799-813, 10.5194/acp-15-799-2015,
601 2015.

602 Platt, U., and Stutz, J: *Differential Optical Absorption Spectroscopy: Principles and*
603 *Applications*, Springer, Berlin., 2008.

604 Ramazan, K. A., Syomin, D., and Finlayson-Pitts, B. J.: The photochemical production of
605 HONO during the heterogeneous hydrolysis of NO₂, *Phys. Chem. Chem. Phys.*, 6, 3836-
606 3843, 10.1039/b402195a, 2004.

607 Ramazan, K. A., Wingen, L. M., Miller, Y., Chaban, G. M., Gerber, R. B., Xantheas, S. S.,
608 and Finlayson-Pitts, B. J.: New experimental and theoretical approach to the heterogeneous
609 hydrolysis of NO₂: Key role of molecular nitric acid and its complexes, *J. Phys. Chem. A*,
610 110, 6886-6897, 10.1021/jp056426n, 2006.

611 Reed, C., Evans, M.J., Crilley, L.R., Bloss, W.J., Sherwen, T., Read, K.A., Lee, J.D., and
612 Carpenter, L.J.: Evidence for renoxification in the tropical marine boundary layer, *Atmos.*
613 *Chem. Phys.*, 17, 4081–4092, 2017.

614 Ridley, B., Ott, L., Pickering, K., Emmons, L., Montzka, D., Weinheimer, A., Knapp, D.,
615 Grahek, F., Li, L., Heymsfield, G., McGill, M., Kucera, P., Mahoney, M. J., Baumgardner,
616 D., Schultz, M., and Brasseur, G.: Florida thunderstorms: A faucet of reactive nitrogen to
617 the upper troposphere, *J. Geophys. Res.-Atmos.*, 109, 2004.

618 Shetter, R. E., Cinquini, L., Lefer, B. L., Hall, S. R., and Madronich, S.: Comparison of
619 airborne measured and calculated spectral actinic flux and derived photolysis frequencies
620 during the PEM Tropics B mission, *J. Geophys. Res.-Atmos.*, 108, 2002.

621 Stemmler, K., Ammann, M., Donders, C., Kleffmann, J., and George, C.: Photosensitized
622 reduction of nitrogen dioxide on humic acid as a source of nitrous acid, *Nature*, 440, 195-
623 198, 10.1038/nature04603, 2006.

624 Stemmler, K., Ndour, M., Elshorbany, Y., Kleffmann, J., D'Anna, B., George, C., Bohn, B.,
625 and Ammann, M.: Light induced conversion of nitrogen dioxide into nitrous acid on
626 submicron humic acid aerosol, *Atmos. Chem. Phys.*, 7, 4237-4248, 2007.

627 Stein, A. F., Draxler, R. R., Rolph, G. D., Stunder, B. J. B., Cohen, M. D., and Ngan, F.:
628 NOAA's HYSPLIT atmospheric transport and dispersion modeling system. *Bul. Amer.*
629 *Meteorol. Soc.*, 96, 2059-2077, 10.1175/BAMS-D-14-00110.1, 2015.

630 Stutz, J., Alicke, B., and Neftel, A.: Nitrous acid formation in the urban atmosphere: Gradient
631 measurements of NO₂ and HONO over grass in Milan, Italy, *J. Geophys. Res.-Atmos.*,
632 107, Artn 8192,10.1029/2001jd000390, 2002.

633 Stutz, J., Oh, H. J., Whitlow, S. I., Anderson, C., Dibbb, J. E., Flynn, J. H., Rappengluck, B.,
634 and Lefer, B.: Simultaneous DOAS and mist-chamber IC measurements of HONO in
635 Houston, TX, *Atmos. Environ.*, 44, 4090-4098, 2010.

636 Su, H., Cheng, Y. F., Oswald, R., Behrendt, T., Trebs, I., Meixner, F. X., Andreae, M. O.,
637 Cheng, P., Zhang, Y., and Poschl, U.: Soil Nitrite as a Source of Atmospheric HONO and
638 OH Radicals, *Science*, 333, 1616-1618, 10.1126/science.1207687, 2011.

639 Trentmann, J., Andreae, M. O., and Graf, H. F.: Chemical processes in a young biomass-
640 burning plume, *J. Geophys. Res.-Atmos.*, 108, 2003.

641 VandenBoer, T. C., Brown, S. S., Murphy, J. G., Keene, W. C., Young, C. J., Pszenny, A. A.
642 P., Kim, S., Warneke, C., de Gouw, J. A., Maben, J. R., Wagner, N. L., Riedel, T. P.,
643 Thornton, J. A., Wolfe, D. E., Dube, W. P., Ozturk, F., Brock, C. A., Grossberg, N., Lefer,
644 B., Lerner, B., Middlebrook, A. M., and Roberts, J. M.: Understanding the role of the
645 ground surface in HONO vertical structure: High resolution vertical profiles during
646 NACHTT-11, *J. Geophys. Res.-Atmos.*, 118, 10155-10171, 2013.

647 VandenBoer, T. C., Markovic, M. Z., Sanders, J. E., Ren, X., Pusede, S. E., Browne, E. C.,
648 Cohen, R. C., Zhang, L., Thomas, J., Brune, W. H., and Murphy, J. G.: Evidence for a
649 nitrous acid (HONO) reservoir at the ground surface in Bakersfield, CA, during CalNex
650 2010, *J. Geophys. Res.-Atmos.*, 119, 9093-9106, 10.1002/2013JD020971, 2014.

651 VandenBoer, T. C., Young, C. J., Talukdar, R. K., Markovic, M. Z., Brown, S. S., Roberts, J.
652 M., and Murphy, J. G.: Nocturnal loss and daytime source of nitrous acid through reactive
653 uptake and displacement, *Nature Geosci.*, 8, 55-60, 2015.

654 VandenBoer, T.C., Brown, S.S., Murphy, J.G., Keene, W.C., Young, C.J., Pszenny, A.A.P.,
655 Kim, S., Warneke, C., Gouw, Joost de, Maben, J.R., Wagner, N.L., Riedel, T.P., Thornton,
656 J.A., Wolfe, D.E., Dube, W.P., Ozturk, F., Brock, C.A., Grossberg, N., Lefer, B., Lerner,
657 B., Middlebrook, A.M., and Roberts, J.M.: Understanding the role of the ground surface in
658 HONO vertical structure: High resolution vertical profiles during NACHTT-11, *J.*
659 *Geophys. Res.-Atmos.*, 118, 10,155–10,171, doi:10.1002/jgrd.50721, 2013.

660 Villena, G., Kleffmann, J., Kurtenbach, R., Wiesen, P., Lissi, E., Rubio, M. A., Croxatto, G.,
661 and Rappengluck, B.: Vertical gradients of HONO, NO_x and O₃ in Santiago de Chile,
662 Atmos. Environ., 45, 3867-3873, 2011.

663 Wong, K. W., Oh, H. J., Lefer, B. L., Rappengluck, B., and Stutz, J.: Vertical profiles of
664 nitrous acid in the nocturnal urban atmosphere of Houston, TX, Atmos. Chem. Phys., 11,
665 3595-3609, 2011.

666 Wong, K. W., Tsai, C., Lefer, B., Haman, C., Grossberg, N., Brune, W. H., Ren, X., Luke,
667 W., and Stutz, J.: Daytime HONO vertical gradients during SHARP 2009 in Houston, TX,
668 Atmos. Chem. Phys., 12, 635-652, 2012.

669 Wong, K. W., Tsai, C., Lefer, B., Grossberg, N., and Stutz, J.: Modeling of daytime HONO
670 vertical gradients during SHARP 2009, Atmos. Chem. Phys., 13, 3587-3601, 2013.

671 Wu, C., and Yu, J.Z.: Evaluation of linear regression techniques for atmospheric applications:
672 the importance of appropriate weighting, Atmos. Meas. Tech., 11, 1233–1250, 2018.

673 Ye, C. X., Zhou, X. L., Pu, D., Stutz, J., Festa, J., Spolaor, M., Cantrell, C., Mauldin, R. L.,
674 Weinheimer, A., and Haggerty, J.: Comment on "Missing gas-phase source of HONO
675 inferred from Zeppelin measurements in the troposphere", Science, 348,
676 10.1126/science.aaa1992, 2015.

677 Ye, C. X., Gao, H. L., Zhang, N., and Zhou, X.: Photolysis of nitric Acid and nitrate on
678 natural and artificial surfaces, Environ. Sci. Technol., 50, 3530-3536, 2016a.

679 Ye, C. X., Zhou, X. L., Pu, D., Stutz, J., Festa, J., Spolaor, M., Tsai, C., Cantrell, C., Mauldin,
680 R. L., Campos, T., Weinheimer, A., Hornbrook, R. S., Apel, E. C., Guenther, A., Kaser, L.,
681 Yuan, B., Karl, T., Haggerty, J., Hall, S., Ullmann, K., Smith, J. N., Ortega, J., and Knote,
682 C.: Rapid cycling of reactive nitrogen in the marine boundary layer, Nature, 532, 489-491,
683 2016b.

684 Ye, C., Zhang, N., Gao, H., and Zhou, X.: Photolysis of particulate nitrate as a source of
685 HONO and NO_x, Environ Sci Technol, DOI: 10.1021/acs.est.7b00387, 2017.

686 Young, C.J., Washenfelder, R.A., Roberts, J.M., Mielke, L.H., Osthoff, H.D., Tsai, C.,
687 Pikelnaya, O., Stutz, J., Veres, P.R., Cochran, A.K., VandenBoer, T.C., Flynn, J.,
688 Grossberg, N., Haman, C.L., Lefer, B., Stark, B., Martin, G., Gouw, Joost de., Gilman, J.B.,
689 Kuster, W.C., and Brown, S.S.: Vertically Resolved Measurements of Nighttime Radical
690 Reservoirs in Los Angeles and Their Contribution to the Urban Radical Budget, Environ.
691 Sci. Technol., 46 (20), 10965–10973, 2012.

692 Zhang, N., Zhou, X., Shepson, P. B., Gao, H., Alaghmand, M., and Stirm, B.: Aircraft
693 measurement of HONO vertical profiles over a forested region, *Geophys. Res. Lett.*, 36,
694 Artn L15820,10.1029/2009gl038999, 2009.

695 Zhang, N., Zhou, X., Bertman, S., Tang, D., Alaghmand, M., Shepson, P. B., and Carroll, M.
696 A.: Measurements of ambient HONO concentrations and vertical HONO flux above a
697 northern Michigan forest canopy, *Atmos. Chem. Phys.*, 12, 8285-8296, 2012.

698 Zhou, X., Civerolo, K., Dai, H., Huang, G., Schwab, J., and Demerjian, K.: Summertime
699 nitrous acid chemistry in the atmospheric boundary layer at a rural site in New York State,
700 *J. Geophys. Res.*, 107, doi:10.1029/2001JD001539, 2002.

701 Zhou, X., Gao, H., He, Y., Huang, G., Bertman, S. B., Civerolo, K., and Schwab, J.: Nitric
702 acid photolysis on surfaces in low-NO_x environments: Significant atmospheric
703 implications, *Geophys. Res. Lett.*, 30, Artn 2217,10.1029/2003gl018620, 2003.

704 Zhou, X., Zhang, N., TerAvest, M., Tang, D., Hou, J., Bertman, S., Alaghmand, M., Shepson,
705 P. B., Carroll, M. A., Griffith, S., Dusanter, S., and Stevens, P. S.: Nitric acid photolysis on
706 forest canopy surface as a source for tropospheric nitrous acid, *Nature Geosci.*, 4, 440-443,
707 10.1038/NGEO1164, 2011.

708 Zhu, C. Z., Xiang, B., Zhu, L., and Cole, R.: Determination of absorption cross sections of
709 surface-adsorbed HNO₃ in the 290-330 nm region by Brewster angle cavity ring-down
710 spectroscopy, *Chem. Phys. Lett.*, 458, 373-377, 2008.

711
712

713 Table 1. Measurements from the NOMADSS 2013 summer study used in this analysis.

Parameters	Instrument	Time Resolution	Detection Limit	Accuracy	References
HONO	LPAP	200 s	1 pptv	20%	(1, 2)
pNO₃	LPAP	360 s	2 pptv	30%	(1, 2, 3)
HNO₃	LPAP	20 min	2 pptv	30%	(1, 2, 3)
NO	CI	1 s	20 pptv	10%	(4)
NO₂	CI	1 s	40 pptv	15%	(4)
O₃	CI	1 s	100 pptv	5%	(4)
OH	SICIMS	30 s	*5×10 ⁴	30%	(5, 6)
HONO	DOAS	60 s	~ 30 pptv	20%	(7)
Photolysis Frequencies	CAFS	6 s		10-15%	(8)
Surface area density	SMPS/UHSAS	65 s/1 s		20%	(9)
VOCs	PTRMS	15 s		20%	(10, 11)
VOCs/organic nitrates	TOGA	20 s		20%	(12)

714 *in molecules cm⁻³

715 LPAP: long-path absorption photometric (LPAP) systems

716 CI: 4-channel chemiluminescence instrument

717 SICIMS: selected-ion chemical-ionization mass spectrometer

718 DOAS: Differential Optical Absorption Spectroscopy

719 CAFS: Charged-coupled device Actinic Flux Spectroradiometer

720 SMPS: Scanning Mobility Particle Sizer

721 UHSAS: Ultra-High Sensitivity Aerosol Spectrometer

722 PTRMS: Proton Transfer Reaction Mass Spectrometry

723 TOGA: Trace Organic Gas Analyzer

724 References: (1) Zhang et al., 2012; (2) Ye et al., 2016b; (3) Huang et al., 2002; (4) Ridley et

725 al., 2004; (5) Hornbrook et al., 2011b; (6) Mauldin et al., 2010; (7) Platt and Stutz, 2008;

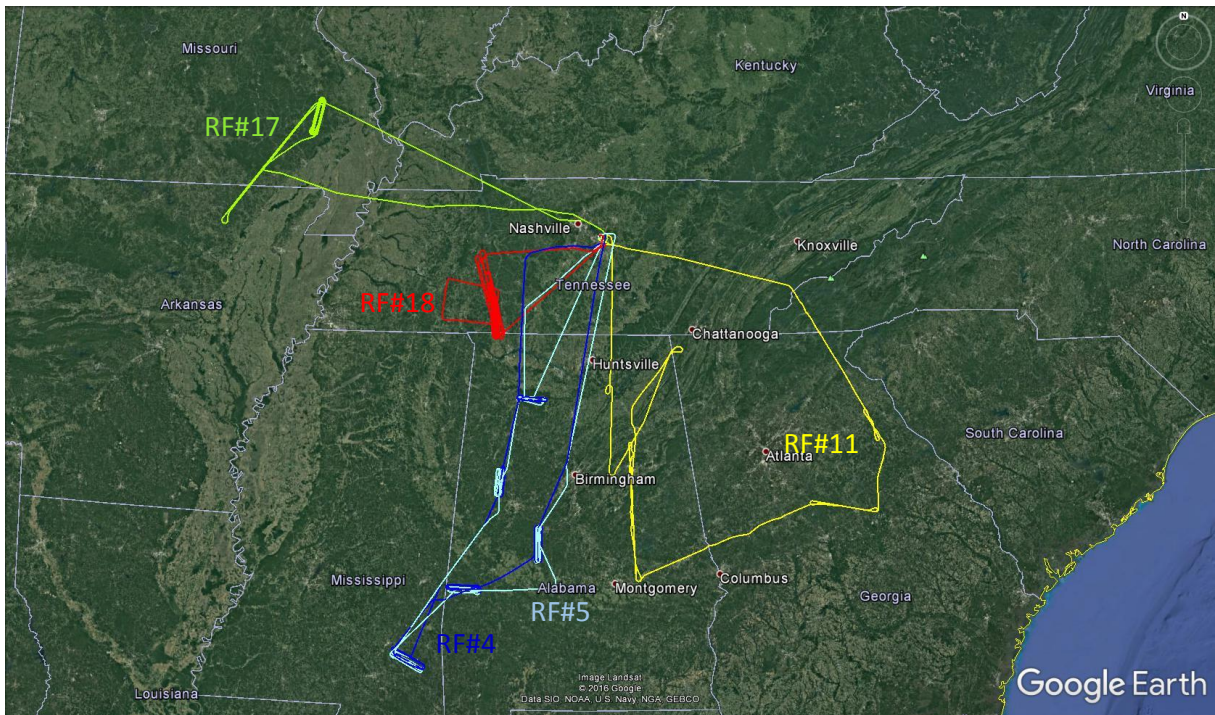
726 (8) Shetter et al., 2002; (9) Flagan, 2011; (10) Karl et al., 2003; (11) de Gouw and

727 Warneke, 2007; (12) Hornbrook et al., 2011a.

728 Table 2. Data statistics for HONO, NO_x and pNO₃ measurements both in the PBL and the FT
 729 from the five Southeast U.S. research flights during the NOMADSS 2013 summer field study.
 730 The statistics analysis is based on 1-min NO_x data, 3-min HONO data and 6-min pNO₃ data.
 731

		HONO, pptv	NO_x, pptv	pNO₃, pptv
PBL	Range	3.1 – 34.4	81 – 1774	9 – 186
	Mean ± SD	11.2 ± 4.3	316 ± 182	76 ± 45
	Median	10.3	279	66
	N	356	904	121
FT	Range	1.3 - 15.2	<10 – 582	3 – 179
	Mean ± SD	5.6 ± 3.4	94 ± 53	35 ± 39
	Median	4.2	92	15
	N	157	655	46

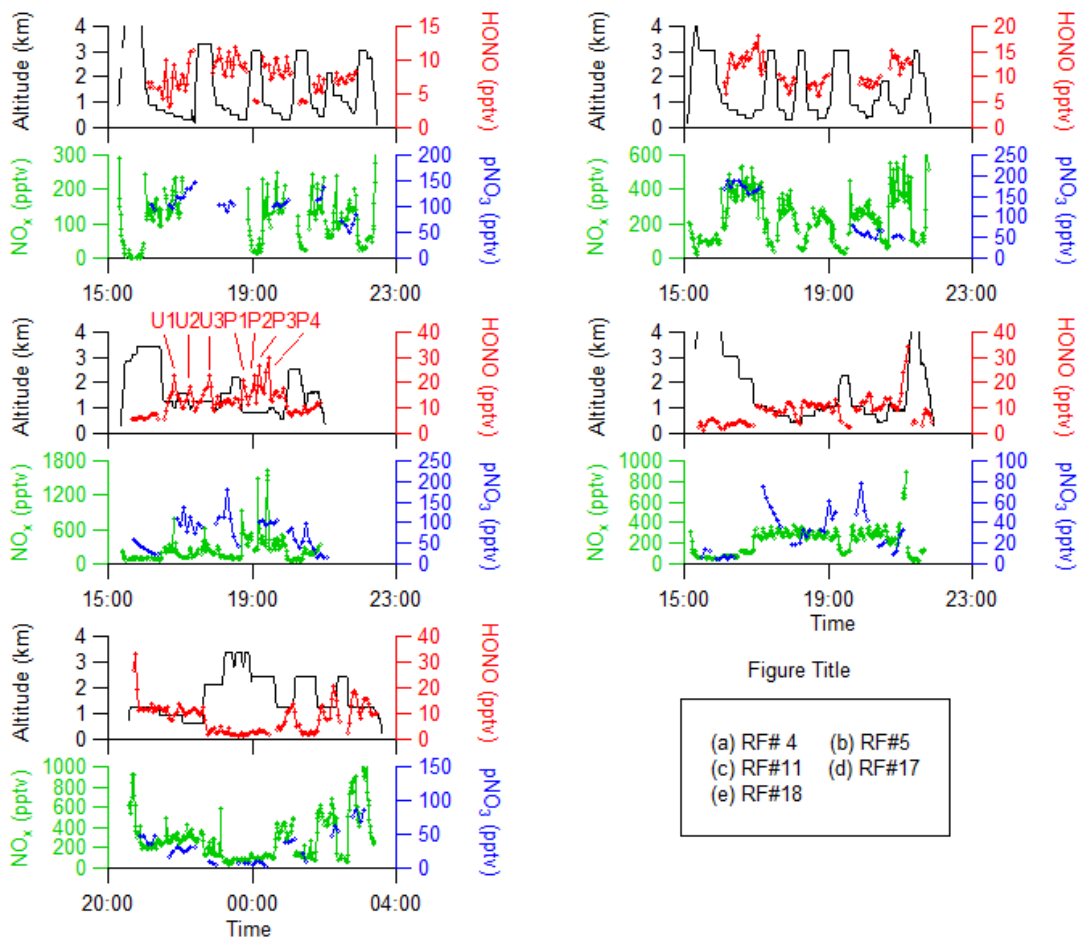
732



733

734 Figure 1. Flight tracks in the Southeast US during the NOMADSS 2013 summer study. The
 735 flight start time and end time in UTC (= EDT+4) are: RF#4 (blue): 15:12 and 22:30, June 12,
 736 2013; RF#5 (light blue): 15:04 and 21:52, June 14, 2013; RF#11 (yellow): 15:20 and 21:02,
 737 June 29, 2013; RF#17 (green): 15:07 and 21:57, July 11, 2013; RF#18 (red): 20:32, July 12,
 738 2013, and 03:37, July 13, 2013.

739

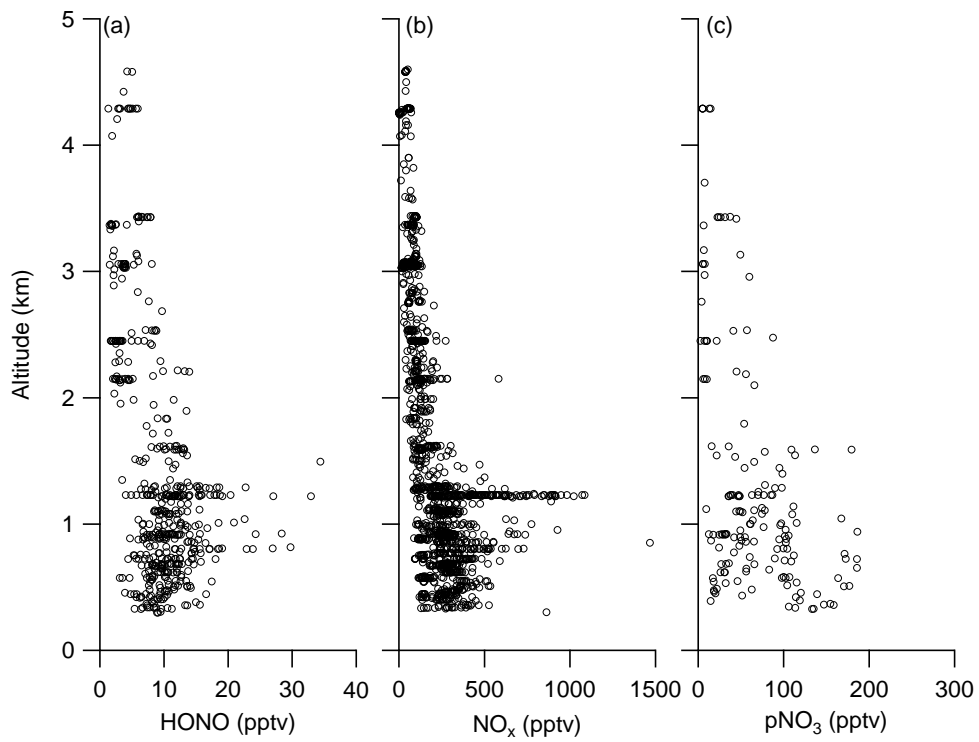


740

741

742 Figure 2. Time series of altitude, HONO, NO_x and pNO₃ in five flights (RF #4, RF #5, RF
 743 #11, RF #17 and #18) in the Southeast US during the NOMADSS 2013 summer study. In RF
 744 #11, the plumes U1 and U3 were from Birmingham, AL; the plume U2 was from
 745 Montgomery, AL; the plumes P1-P3 were from a power plant in Monroe County, GA; and the
 746 plume P4 was from a power plant in Putnam country, GA.

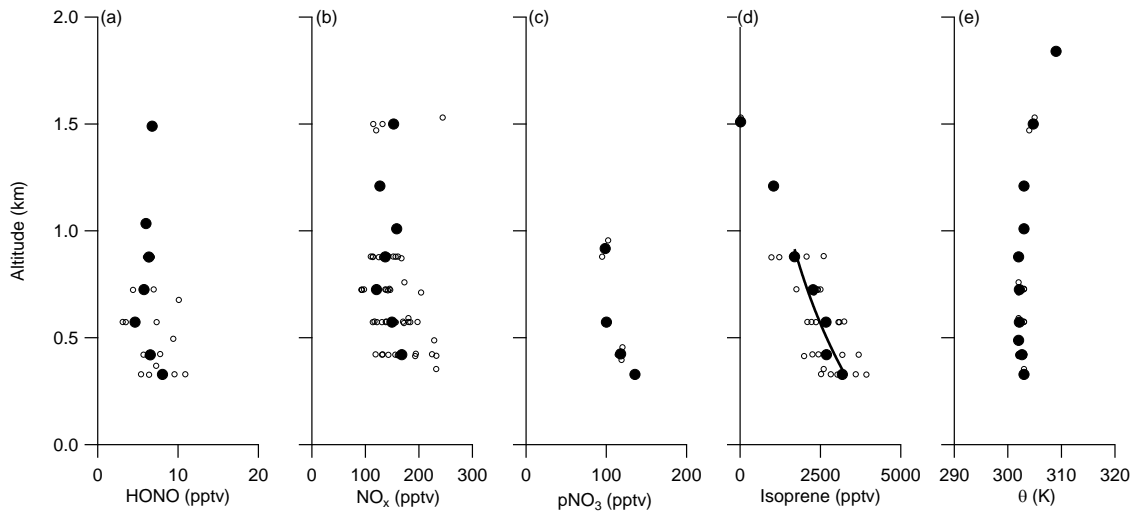
747



748

749 Figure 3. Vertical distributions of concentrations of HONO (a), NO_x (b), and pNO₃ (c) in the
750 five selected flights in the Southeast US during the NOMADSS 2013 summer study.

751

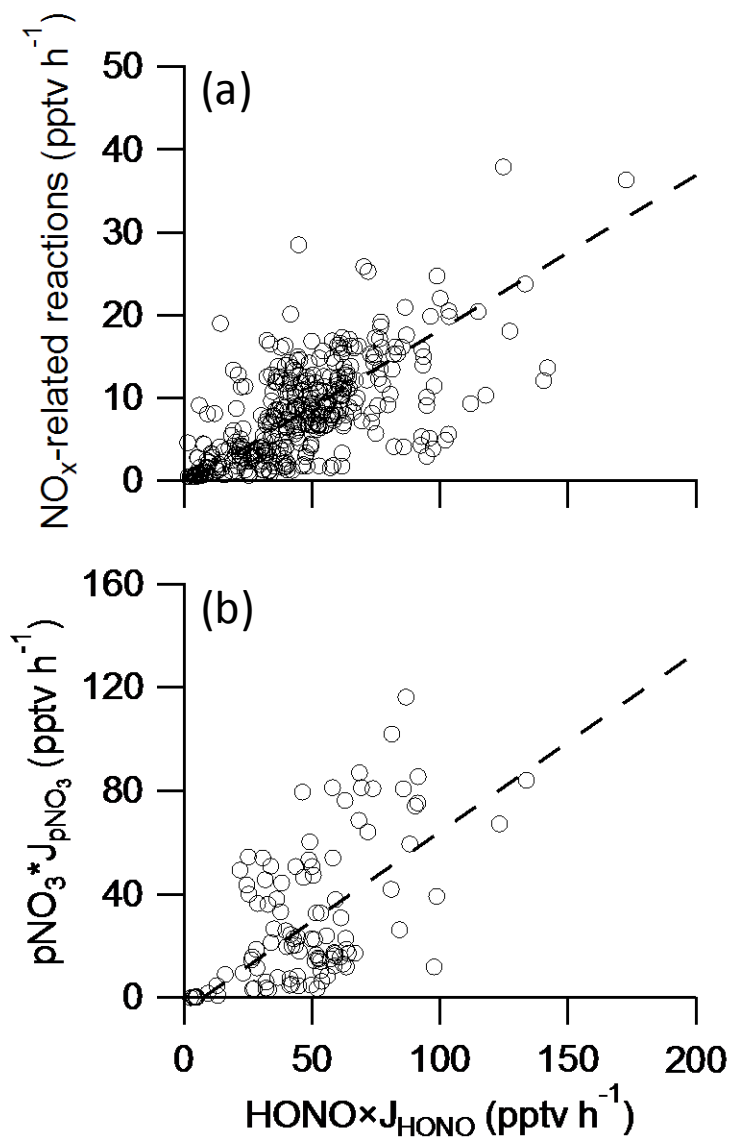


753

754 Figure 4. Vertical distributions of concentrations of HONO (a), NO_x (b), pNO₃ (c), isoprene
 755 (d) and potential temperature (e) in the PBL during the first race-track of RF#4 from 11:00 –
 756 12:15 LT (16:00 – 17:15 UTC), June 12, 2013. The small open circles represent the 1-min
 757 data points, the large solid circles the mean values for each race-track measurement altitude.

758 The line in (d) is the best fit of (Eq. 1) to the isoprene data: $C = 4700e^{-h/0.895}$, $r^2 = 0.93$.

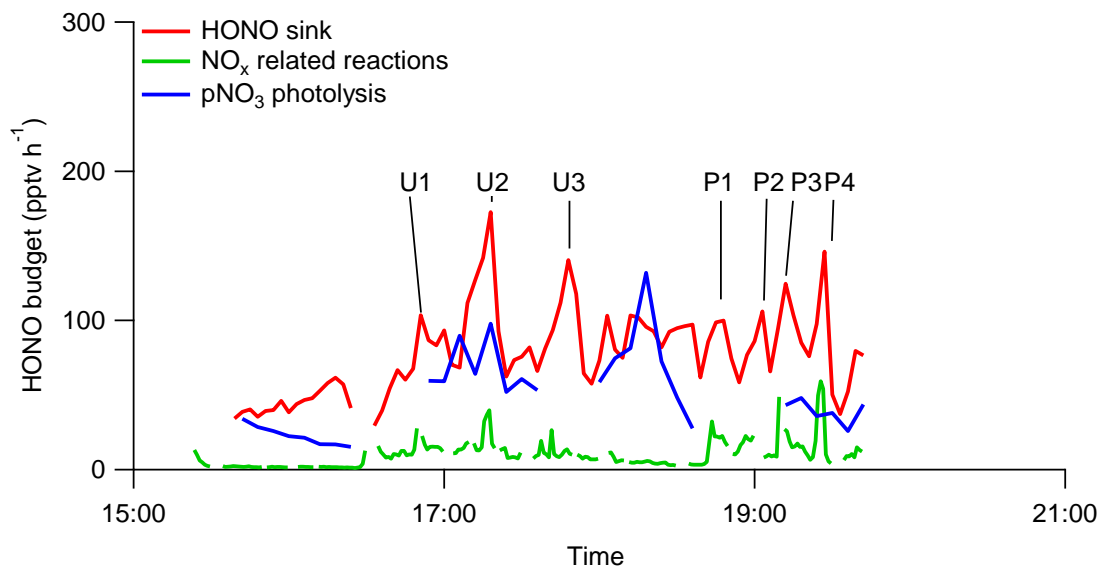
759



760

761 Figure 5. Correlation analysis of main HONO sink (“ $\text{HONO} \times \text{J}_{\text{HONO}}$ ”) with contribution from
 762 NO_x related reactions (a) and with contribution from particulate nitrate photolysis,
 763 $\text{pNO}_3 \times \text{J}_{\text{pNO}_3}$ (b) in the southeast US during the NOMADSS 2013 summer study. The line
 764 represents the Deming least-squares regression (Wu and Yu, 2018) ($r^2=0.40$, intercept = -0.51
 765 and slope = 0.19 for Figure 6a; $r^2=0.34$, intercept = -5.0 and slope = 0.69 for Figure 6b).

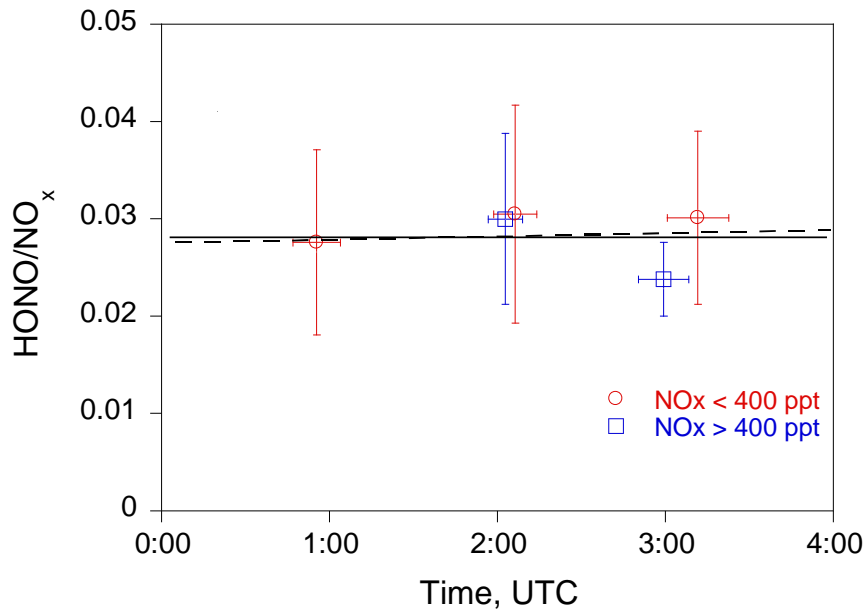
766



768

769 Figure 6. HONO budget analysis in RF #11 in the Southeast US during the NOMADSS 2013
 770 summer study. “HONO sink” is the HONO loss rate contributed by photolysis and the
 771 reaction of HONO with OH radicals, “NO_x related reactions” is the sum of HONO production
 772 rates from all known NO_x reactions, and “pNO₃ photolysis” is the HONO production rate
 773 from photolysis of pNO₃. The calculations are based on 1-min NO_x data, 3-min HONO data
 774 and 6-min pNO₃ data.

775



776

777 Figure 7. The evolution of HONO/NO_x ratio in the nocturnal boundary layer during the
 778 RF#18. The red circles and blue squares are the median HONO/NO_x values under the
 779 conditions of NO_x ≤ 400 pptv and NO_x > 400 pptv, respectively. The horizontal bars indicate
 780 the averaging time periods and the vertical bars the one standard deviation of HONO/NO_x
 781 ratios. The solid line is the least squared fit to the data, and the dashed line indicates a slope
 782 of $3 \times 10^{-4} \text{ hr}^{-1}$. The sunset time at the sampling location was 0:40 UTC.

783